Journal Name

COMMUNICATION

Improving charge injection and charge transport in CuO-based *p*-type DSSCs – A quick and simple precipitation method for small CuO nanoparticles

Received 00th January 20xx,
Accepted 00th January 20xx

DOI: 10.1039/x0xx00000x

www.rsc.org/

Oliver Langmar,[a] Carolina Ganivet,[b] Peter Schol,[a] Tobias Scharl,[a] Gema de la Torre,[b] Tomás Torres,[b,c] Ruben D. Costa,[a,d,*] and Dirk M. Guldi [a,*]

Herein, we introduce a co-precipitation synthesis of CuO, which produces small and uniform nanoparticles (~ 12 nm) with a specific surface area of 97.3 m^2/g. The resulting CuO nanoparticles are superior to the commercial ones, which have previously been used to prepare *p*-type DSSCs. In turn, we compared *p*-type DSSCs consisting of CuO-based photocathodes based on newly synthesized and commercial nanoparticles. Devices based on newly synthesized CuO nanoparticles enable higher dye loadings, and, in turn, superior short-circuit current densities and efficiencies. To corroborate our findings, electrochemical impedance spectroscopy and intensity modulated photocurrent spectroscopy assays were conducted, revealing a better charge injection and faster charge transport for those photocathodes featuring the newly synthesized CuO nanoparticles.

Introduction

Dye-sensitized solar cells (DSSCs) have long proven to be a viable alternative to crystalline silicon solar cells for solar energy production, due to their low cost and ease of production. In these devices, photons are collected by organic dye molecules which cover a layer of a wide band gap semiconducting material.[1] *n*-Type DSSCs are based on photoanode materials such as titanium(IV) oxide (TiO_2) or zinc(II) oxide (ZnO), while nickel(II) oxide (NiO) is mainly employed in *p*-type DSSCs.[2] Investigations regarding *p*-type DSSCs are largely limited by the lack of suitable alternatives to NiO photocathode materials and the rather poor efficiency of *p*-type DSSCs. In particular, the efficiency of *p*-type DSSCs is at least one order of magnitude inferior to that of *n*-type DSSCs.[3] The consequences are drastic when turning to tandem-DSSCs (*t*-DSSC), where photoinactive, non-transparent platinum counter-electrodes (Pt-CE) used in *n*-type DSSCs are replaced by a *p*-type DSSC. A complementary absorption among the two photoelectrodes, that is, photoanode and photocathode, is essential to realize panchromatic absorption across the solar spectrum.[4,5] In *t*-DSSC, either the open-circuit voltage (V_{OC}) or the short-circuit current density (J_{SC}) of both photoelectrodes are accumulative if they are connected in series or in parallel, respectively.[3] Higher V_{OC} and J_{SC} enable surpassing the Shockley-Queisser limit.[1] *t*-DSSCs are applicable in the field of water-splitting:[6] Sun *et al.* have reported on a dye-sensitized tandem photoelectrochemical cell (PEC) that splits water under visible light conditions. Overall, the photocathode is regarded as the real bottleneck *en route* towards higher efficiencies and, in turn, novel and better performing *p*-type semiconductors are highly desirable.

Despite the fact that NiO is the most commonly used material for *p*-type DSSCs, it presents severe drawbacks, such as low conductivity, failure to withstand thick electrodes, and overlapping light absorption.[3] Copper(I) delafossites ($CuXO_2$), where X is either chromium (Cr), gallium (Ga) or aluminum (Al), have emerged in recent years as a viable alternative to NiO due to their higher conductivities, excellent transmission features, and shifted valence band (VB) energies. Although higher V_{OC} are typically noted for $CuXO_2$ based *p*-type DSSCs,[7] the following facts should not be neglected: On one hand, hydrothermal or high temperature solid-state syntheses of $CuXO_2$ are expensive and, on the other hand, the relatively large particle sizes of $CuXO_2$ (typically ≤ 100 nm) limit loadings of the photosensitizer.[7] It is surprising that the use of copper(II) oxide (CuO) has been underrated. CuO-based films reveal VB energies comparable to those of NiO, but higher conductivities and charge carrier mobilities.[8–10] A proof-of-concept regarding CuO as photocathode material in *p*-type DSSCs was presented by Sumikura *et al.*, but the efficiency was rather moderate with 0.01%.[11] Recently, we have revisited the use of CuO in *p*-type

[a] *Department of Chemistry and Pharmacy, Interdisciplinary Center for Molecular Materials, University of Erlangen-Nürnberg, Egerlandstr. 3, 91058 Erlangen, Germany.*
[b] *Universidad Autónoma de Madrid, c/Francisco Tomás y Valiente 7, 28049 Madrid, Spain.*
[c] *Instituto Madrileño de Estudios Avanzados (IMDEA)-Nanociencia c/ Faraday, 9, Cantoblanco, 28049 Madrid, Spain.*
[d] *Instituto Madrileño de Estudios Avanzados (IMDEA)-Materiales, c/Eric Kandel, 2, Tecnogetafe, 28906 Getafe, Madrid, Spain*

† Footnotes relating to the title and/or authors should appear here.
Electronic Supplementary Information (ESI) available: [details of any supplementary information available should be included here]. See DOI: 10.1039/x0xx00000x

based DSSCs and have realized efficiencies of 0.10% and 0.19% using electron-accepting phthalocyanines in combination with iodine- and cobalt-electrolytes, respectively.[12,13] Key factors were the calcination temperature, the electrode thickness, and the I^-/I_2 ratio in the electrolyte. Still, from electrochemical impedance spectroscopy (EIS) experiments, we concluded that one of the major bottlenecks is the high charge injection resistance.

In the present work, we focus on a new approach to improve charge injection properties by preparing small CuO nanoparticles (~ 12 nm) via a simple precipitation method. As a reference, we used commercially available CuO (com-CuO), which has been used at this point in time. Small particle sizes and high surface areas of the newly synthesized CuO (syn-CuO) and their respective mesoporous films are beneficial for improving the J_{SC} and the efficiency of *p*-type DSSCs by 60% and a factor of 1.5, respectively, relative to com-CuO.

Results

Syn-CuO nanoparticles (NP) were prepared by means of modified precipitation synthesis reported by Zhu *et.al.*.[14] Here an aqueous solution of copper(II)acetate with small amounts of glacial acetic acid was heated to 65°C under vigorous stirring. Upon reaching the target temperature, sodium hydroxide was swiftly added, which rapidly lead to the formation of copper(II)hydroxide, as indicated by the formation of a blueish precipitate. Further stirring at 65°C for several minutes yielded the dark-brown/black syn-CuO NPs. For a more detailed description of the synthesis procedure, please see the SI. X-ray diffraction (XRD) assays confirmed the monoclinic crystal structure of syn- and com-CuO powder samples, and their respective electrodes calcinated at 300°C - **Figure 1**.[8] Powder samples feature crystallite sizes of 9.4 (com- CuO) and 7.8 nm (syn-CuO), while films consisted of crystallites of 13.3- and 13.6 nm-sized com-CuO and syn-CuO, respectively – **Table 1**.[15]

Transmission electron microscopy (TEM) revealed similar rod-like morphologies for com-CuO and syn-CuO, while the particle sizes differed greatly with 55.7 ± 20.5 nm (com-CuO) and 12.1 ± 3.4 nm (syn-CuO) – **Figure 2**. Scanning electron microscopy (SEM) assays of the calcinated electrodes further supported the increase in particle size upon calcination – **Figure 2**. The electrode surface of syn-CuO-based electrodes is more homogenous with smaller particle sizes of 19.6 ± 4.3 nm compared to 53.4 ± 19.0 nm for electrodes based on com-CuO NPs - **Table 1**.

From XRD, TEM, and SEM studies we conclude that the crystallite/particle sizes of syn-CuO and their respective electrodes is smaller than that of com-CuO. In turn, a higher specific surface area and a higher uptake of the photosensitizer are likely to evolve. Brunauer–Emmett–Teller (BET) measurements on the respective powder samples revealed specific surface areas of 43.7 m^2/g for com-CuO and 97.3 m^2/g for syn-CuO – **Figure S3**. BET measurements performed on the calcinated electrodes afforded, however, meaningless results due to large error margins. In this sense we turned to dye desorption experiments to gain complementing information about the surface area of the mesoporous photocathodes (*vide infra*)

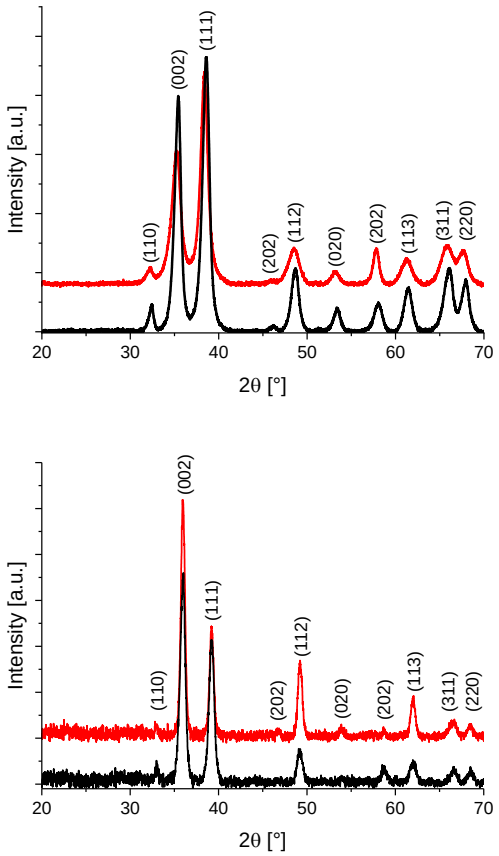

Figure 1: X-ray diffraction patterns of powder samples (top) and electrodes annealed at 300°C (bottom) for com-CuO (black) and syn-CuO (red) with the corresponding crystal planes in parentheses.

Final insights into the electronic structure of the fabricated electrodes came from diffuse reflectance and Kelvin Probe Force Microscopy (KPFM) assays. In line with previous work, the band-gap energies (E_g) were determined as 1.73 and 1.82 eV for com-CuO and syn-CuO based electrodes, respectively.[12,16] Compared to NiO-based photocathodes, which show high transparencies due to the wide bandgap nature of NiO, our newly developed syn-CuO based photocathodes show extended absorptions of the electrode up to the long wavelength region of the solar spectrum – **Figure S1**.

Table 1: Crystallite sizes determined by XRD, particle sizes determined by TEM as well as SEM, BET surface areas, band gap energies (E_g), and Fermi-Level energies (E_F) of com-CuO and syn CuO.

CuO-NP	Crystallite size [nm]		Particle size [nm]		BET surface area [m^2/g]	E_g [eV]	E_F vs. NHE [V][a)]
	XRD powder	XRD film	TEM powder	SEM film			
com-CuO	9.4	13.3	55.7 ± 20.5	53.4 ± 19.0	43.7	1.73	0.55 ± 0.02
syn-CuO	7.8	13.6	12.1 ± 3.4	19.6 ± 4.3	97.3	1.82	0.58 ± 0.03

a) E_F referenced vs. standard hydrogen electrode (NHE), determined from an average of three CuO-based electrodes.

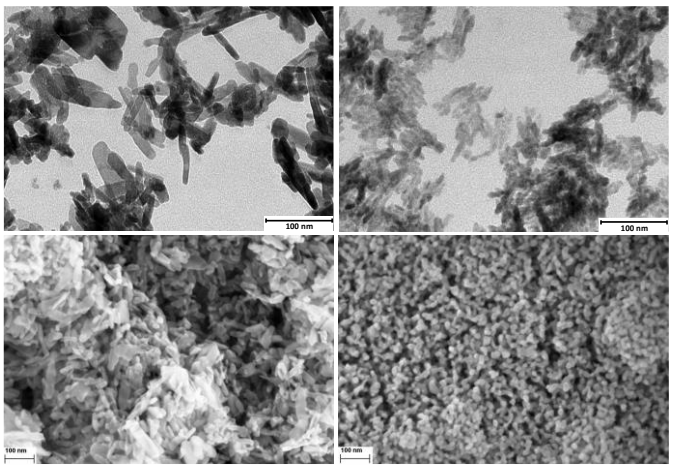

Figure 2: TEM images of powder samples (top) and SEM images of calcinated electrodes (bottom) of com-CuO (left) and syn-CuO (right).

Nevertheless by sensitizing syn-CuO photocathodes with our recently developed electron-accepting zinc(II)phthalocyanine (**ZnPc1**), reasonable light-harvesting properties of the respective photosensitizer evolve in the low-energy region of the solar spectrum.[12] As recently outlined by Odobel *et.al.* this underlines the notion that CuO can be applied as suitable photocathode material for p-DSSCs, especially in conjunction with low-energy photosensitizer.[17] Moreover, Fermi-level energies (E_F) of 0.55 ± 0.02 V vs. NHE for com-CuO and 0.58 ± 0.03 V vs. NHE for syn-CuO prompt to marginal differences in the driving force for charge injection evolving from the photoexcited photosensitizer and the photocathode.

Devices

In the next step, we assembled 1.7 – 1.8 µm thick CuO-based *p*-type DSSCs consisting of photocathodes based on either com-CuO or syn-CuO and the electron accepting **ZnPc1** - **Figure S4**.[12] The figures-of-merit are shown in **Table 2**, while the current density *vs.* applied voltage curves (J-V) and the incident photon-to-current conversion efficiency spectra (IPCE) are depicted in **Figure 3**.

Figures-of-merit for syn-CuO devices – 89.9 mV (V_{OC}), 3.36 mA/cm² (J_{SC}), and an efficiency (η) of 0.11% – are superior to those for com-CuO devices – 86.5 mV (V_{OC}), 2.02 mA/cm² (J_{SC}), and 0.073% (η). The J_{SC} trend is further corroborated by the IPCE maxima at 670 nm, which corresponds to the photocurrent

Table 2: Device figures-of-merit of *p*-type DSSCs based on com-CuO and syn-CuO as photocathodes.

CuO-NP	V_{oc} [mV]	J_{sc} [mA/cm²]	FF	η [%]	IPCE [%] at 670 nm	Thickness [µm]	Dye loading [mol/cm²][a)]
com-CuO	86.5	2.02	0.41	0.073	15.9	1.7	1.66 ± 0.74
syn-CuO	89.9	3.36	0.36	0.11	27.9	1.8	4.91 ± 0.15

a) all values multiplied by 10^{-9} and determined from an average of five sensitized electrodes.

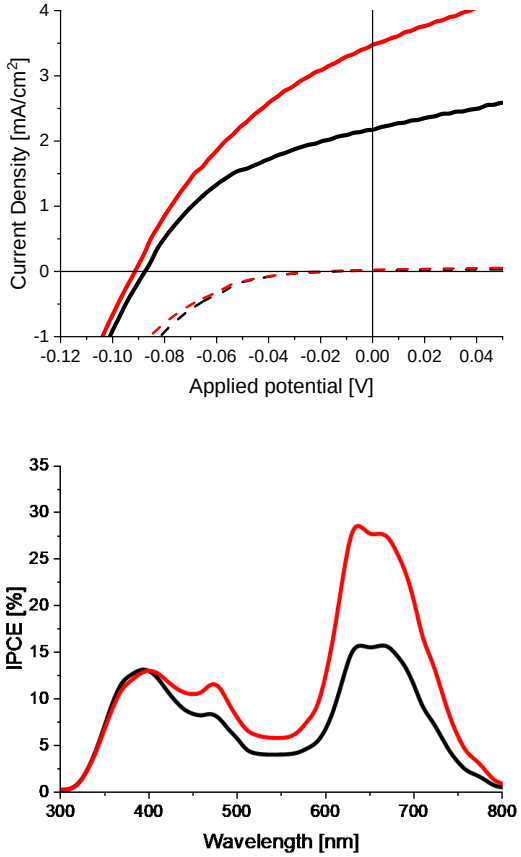

Figure 3: J-V curves (top) under AM 1.5 conditions (solid lines) and in the dark (dashed lines) and IPCE spectra (bottom) for *p*-type DSSCs with com-CuO (black) or syn-CuO (red) based photocathodes.

produced by **ZnPc1**, of 27.9% (syn-CuO) and 15.9% (com-CuO). Furthermore, the IPCEs only point to minor contributions to the total photocurrent due to the photoexcitation of CuO and the I^-/I_3^- redox couple, a fact that was also observed by Odobel *et.al.* for p-DSSCs based on CuO nanorods.[17] By virtue of nearly identical E_g and E_F energies and, therefore, similar charge injection driving forces as well as similar electrode thicknesses, increases in J_{SC} and η might be rationalized by different CuO surface areas. At this point, differences in the charge transport properties between both CuO photoelectrodes can not be ruled out – *vide infra*. From BET and SEM assays of the powder samples and annealed electrodes, which reveal higher surface areas for syn-CuO than for com-CuO, we infer higher **ZnPc1** loading and, in turn, higher J_{SC}. As a matter of fact, desorption experiments revealed a three times higher **ZnPc1** loading for electrodes based on syn-CuO (4.91 ± 0.15 x 10^{-9} mol/cm²) compared to com-CuO (1.66 ± 0.74 x 10^{-9} mol/cm²) – **Table 2**.

To gain deeper insights into the device mechanism, we turned to EIS, which is an ideal tool to study the reactions across interfaces in devices.[13,18,19] In general, the two semicircles in the high and low frequency region of the Nyquist plots for *p*-type DSSCs relate to the Pt-CE/electrolyte interface and the **ZnPc1**/electrode/electrolyte interface, respectively.[18] Moreover, scanning the voltage range from V_{OC} to J_{SC} conditions enables probing the charge injection in CuO-based *p*-type DSSCs under AM 1.5 conditions.[13] **Figure 4** depicts the charge transfer

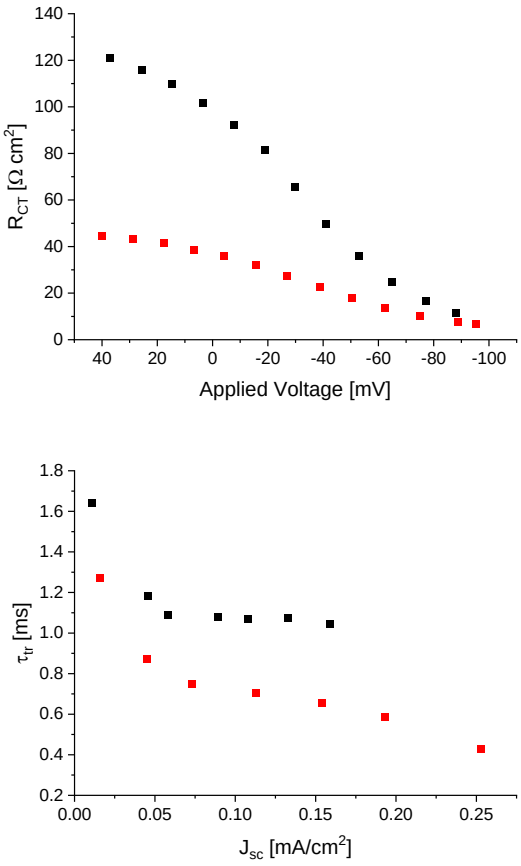

Figure 4: R_{CT} vs. applied voltage (top) and τ_{tr} vs. J_{SC} (bottom) for *p*-type DSSCs consisting of com-CuO (black) or syn-CuO (red) based photocathodes.

resistance (R_{CT}) for the p-type DSSCs recorded over the entire voltage range with the calculated diffusion lengths (L_{eff}), diffusion coefficients (D_{eff}), and charge collection efficiencies (η_{CC}) shown in **Figure S5**.[13,19] We hypothesize that a difference in charge injection and / or charge transport is responsible for the main difference in efficiency. Indeed, EIS measurements under AM 1.5 and J_{SC} conditions underline our hypothesis, since R_{CT} is directly related under these conditions to the charge injection due to a lack of recombination – **Figure 4**.[12,13] At J_{SC}, R_{CT} for devices based on syn-CuO (36.5 Ω cm^2) is nearly three times lower than for com-CuO based devices (99.9 Ω cm^2). Notably, the differences in R_{CT} agree well with the different amount of **ZnPc1** loading – *vide supra*. In other words, charge injection increases in *p*-type DSSCs based on syn-CuO by a factor of three due to a superior **ZnPc1** loading. A more efficient charge injection in syn-CuO-based devices is also supported by larger L_{eff}, D_{eff}, and η_{CC} relative to com-CuO based devices – **Figure S5**.

Although differences in the specific surface area, the **ZnPc1** loading and, in turn, the charge injection are identified as the main reasons for increasing J_{SC}s and ηs for syn-CuO based devices when compared to devices fabricated with com-CuO, changes in charge transport inside the photoelectrode material due to traps, etc. might be also the cause for higher J_{SC} and better η. EIS measurements failed, however, to address charge transport aspects, since the Nyquist plots lacked any transmission line features. More informative were the investigations by means of intensity modulated photocurrent spectroscopy (IMPS). IMPS provides valuable insights into transport times (τ_{tr}) inside the photocathodes under varying illumination intensities.[19–21] **Figure 4** shows the dependence of the transport times under different J_{SC} conditions, which is set by varying the LED illumination density, for com- and syn-CuO based devices. At first glance, τ_{tr} increases as a function of decreasing J_{SC} in both cases. A closer analysis reveals, however, that *p*-type DSSCs employing syn-CuO based photocathodes display at ~ 0.15 mA/cm^2 with 0.65 ms a two times faster charge transport than com-CuO based devices with 1.05 ms. In short, not only the superior charge injection but also the improved charge transport of syn-CuO based photocathodes impact J_{SC} and η. It needs to be clarified if fewer traps or a better morphology – just to name a few – of syn-CuO photocathodes account for the better charge transport. This issue will be tackled in future work.

Conclusions

In conclusion, a quick and simple precipitation synthesis was performed to synthesize syn-CuO. Their morphological, energetical and electrical properties have been probed and compared to com-CuO NPs, showing smaller particle sizes and higher specific surface areas in line with equal energetics. Mesoporous films have been prepared from both materials in order to compare their properties as photocathodes in *p*-type DSSCs. Devices prepared from syn-CuO NPs show, to this end, superior efficiencies of 0.11% compared to devices based on com-CuO NPs with only 0.073%. This increase in efficiency is mainly attributed to a superior dye loading of the syn-CuO NPs which goes in hand with an increase in J_{sc} of 60%. EIS and IMPS assays complemented the device characterization showing a higher amount of charge injection and improved charge transport, which correlates well with the increased dye loading and J_{sc}. Future work will focus on the preparation and characterization of novel CuO-based materials for *p*-type DSSC applications.

Conflicts of interest

There are no conflicts to declare.

Acknowledgement

The authors thank the German Science Council (DFG) for the financial support in the framework of the Cluster of Engineering of Advanced Materials (EAM). O.Langmar thanks S. Romeis for the BET measurements.

Notes and references

1 A. Hagfeldt, G. Boschloo, L. Sun, L. Kloo and H. Pettersson, *Chem. Rev.*, 2010, **110**, 6595–6663.

2 F. Odobel, L. Le Pleux, Y. Pellegrinn and E. Blart, *Acc. Chem.*

Res., 2010, **43**, 1063–1071.
3 F. Odobel and Y. Pellegrin, *J. Phys. Chem. Lett.*, 2013, **4**, 2551–2564.
4 A. Nattestad, A. J. Mozer, M. K. R. Fischer, Y. Cheng, A. Mishra, P. Bäuerle and U. Bach, *Nat. Mater.*, 2010, **9**, 31–35.
5 Y. Farré, M. Raissi, A. Fihey, Y. Pellegrin, E. Blart, D. Jacquemin and F. Odobel, *ChemSusChem*, 2017, **10**, 2618–2625.
6 F. Li, K. Fan, B. Xu, E. Gabrielsson, Q. Daniel, L. Li and L. Sun, *J. Am. Chem. Soc.*, 2015, **137**, 9153–9159.
7 M. Yu, T. I. Draskovic and Y. Wu, *Phys. Chem. Chem. Phys.*, 2014, **16**, 5026–5033.
8 D. M. Jundale, P. B. Joshi, S. Sen and V. B. Patil, *J. Mater. Sci. Mater. Electron.*, 2012, **23**, 1492–1499.
9 S. Makhlouf, M. Kassem and M. Abdel-Rahim, *J. Mater. Sci.*, 2009, **44**, 3438–3444.
10 Q. Zhang, K. Zhang, D. Xu, G. Yang, H. Huang, F. Nie, C. Liu and S. Yang, *Prog. Mater. Sci.*, 2014, **60**, 208–237.
11 S. Sumikura, S. Mori, S. Shimizu, H. Usami and E. Suzuki, *J. Photochem. Photobiol. A Chem.*, 2008, **194**, 143–147.
12 O. Langmar, C. R. Ganivet, A. Lennert, R. D. Costa, G. de la Torre, T. Torres and D. M. Guldi, *Angew. Chemie Int. Ed.*, 2015, **54**, 7688–7692.
13 O. Langmar, C. R. Ganivet, G. de la Torre, T. Torres, R. D. Costa and D. M. Guldi, *Nanoscale*, 2016, **8**, 17963–17975.
14 J. Zhu, D. Li, H. Chen, X. Yang, L. Lu and X. Wang, *Mater. Lett.*, 2004, **58**, 3324–3327.
15 A. L. Patterson, *Phys. Rev.*, 1939, **56**, 978–982.
16 C. Y. Chiang, M. H. Chang, H. S. Liu, C. Y. Tai and S. Ehrman, *Ind. Eng. Chem. Res.*, 2012, **51**, 5207–5215.
17 T. Jiang, M. Bujoli-Doeuff, Y. Farré, Y. Pellegrin, E. Gautron, M. Boujtita, L. Cario, S. Jobic and F. Odobel, *RSC Adv.*, 2016, **6**, 112765–112770.
18 Z. Huang, G. Natu, Z. Ji, P. Hasin and Y. Wu, *J. Phys. Chem. C*, 2011, **115**, 25109–25114.
19 Z. Huang, G. Natu, Z. Ji, M. He, M. Yu and Y. Wu, *J. Phys. Chem. C*, 2012, **116**, 26239–26246.
20 J. Krüger, R. Plass, M. Grätzel, P. J. Cameron and L. M. Peter, *J. Phys. Chem. B*, 2003, **107**, 7536–7539.
21 L. Peter and K. Wijayantha, *Electrochim. Acta*, 2000, **45**, 4543–4551.

TOC:

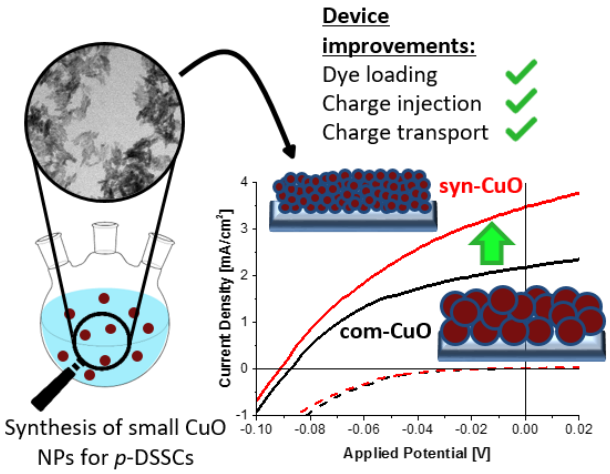

Novel CuO photocathodes based on synthesized nanoparticles achieve superior charge injection and transport properties in p-DSSCs.